Universiteit Antwerpen

The conversion mechanism of amorphous silicon to stoichiometric WS_2

The Conversion Mechanism of Amorphous Silicon to Stoichiometric WS$_2$

Markus H. Heyne[1,2,3,*] Jean-François de Marneffe[3]; Thomas Nuytten[3]; Johan Meersschaut[3]; Thierry Conard[3]; Matty Caymax[3], Iuliana Radu[3]; Annelies Delabie[1,3]; Erik C. Neyts[2]; Stefan De Gendt[1,3]

[1] KU Leuven, Department of Chemistry, Celestijnenlaan 200F, 3001 Leuven, Belgium

[2] University of Antwerp, Department Chemistry, Universiteitsplein 1, 2610 Antwerp, Belgium

[3] Imec, Kapeldreef 75, 3001 Leuven, Belgium

*markus.heyne@gmail.com

Abstract (100 – 250 words)

The deposition of ultra-thin tungsten films and their related 2D chalcogen compounds on large area dielectric substrates by gas phase reactions is challenging. The lack of nucleation sites complicates the adsorption of W-related precursors and subsequent sulfurization usually requires high temperatures. We propose here a technique in which a thin solid amorphous silicon film is used as reductant for the gas phase precursor WF$_6$ leading to the conversion to metallic W. The selectivity of the W conversion towards the underlying dielectric surfaces is demonstrated. The role of the Si surface preparation, the conversion temperature, and Si thickness on the formation process is investigated. Further, the in situ conversion of the metallic tungsten into thin

stoichiometric WS_2 is achieved by a cyclic approach based on WF_6 and H_2S pulses at the moderate temperature of 450 °C, which is much lower than usual oxide sulfurization processes.

Keywords (4 – 6)

2D material, self-aligned deposition, sacrificial conversion, transition-metal dichalcogenide

Introduction

Ultra-thin semiconducting atomic layers such as the transition-metal dichalcogenides (TMDs) WS_2 or MoS_2 show specific properties due to their reduced dimensionality. Monolayers of these TMDs reveal sulfur-terminated basal planes and multilayers are bonded by van der Waals forces, hence, their ideal surface is free of dangling bonds.[1] Due to their lower relative permittivity in comparison to Si, they are also predicted to be more resistant against short-channel effects in field effect transistors and are promising for future scaling in nanoelectronics.[2] Besides this, these materials are promising building blocks in optoelectronics, spintronics, and flexible electronics.[3]–[5] In recent years, much progress on the growth of MX_2 materials has been reported, especially for MoS_2. In comparison to MoS_2, the TMD WS_2 received less attention, despite its higher predicted phonon-limited electron mobility of 700 cm^2/Vs in monolayer due to its lower effective charge carrier mass, in comparison to the value of 440 cm^2/Vs reported for MoS_2.[6]–[8] Those theoretical performances are smaller in real devices due to structural defects such as grain boundaries and

sulfur vacancies, which are occurring as a result of the growth process or post treatment.[9], [10]

A common approach for deposition on large areas is the chemical vapor deposition (CVD) by evaporation of MoO_3 and S supported by Ar/H_2 flow in furnaces with different temperature zones.[11]–[13] This allows the deposition of monolayer triangles with lateral dimensions of a few tens of micron. The crystal orientation can be controlled by using crystalline guiding substrates such as sapphire wafers or GaN films.[14]–[17] Besides of MoO_3, metal halides have been used for deposition as well, since their boiling points are smaller than for the oxides and hence, their vapor transport into processing reactors to the substrate surface is facilitated.[18]–[20] The transition-metal chlorides can be evaporated already below 300 °C and the fluorides are even volatile at room temperature. Besides metal halides, also volatile metal-organic precursors are used to deposit thin films.[21]–[24] Those CVD methods can yield large MX_2 grains, if the nucleation starts from one nucleation point and extends laterally to form the characteristic triangles. Next to the CVD methods, also conversion reactions have been widely investigated. In such reactions, pre-deposited metallic or metal-oxide layers are sulfurized in evaporated elemental sulfur or H_2S.[25] However, sulfurization results in much smaller grain size than CVD for a given temperature, since sulfurized films are initially nanocrystalline and need high recrystallization temperatures to enable grain boundary migration.

The majority of studies were done for MoS_2 due to the ease of fabrication by co-evaporation of MoO_3 (melting point at 795 °C) and sulfur in tube furnaces and the MoS_2 deposition directly from the gas phase. [6], [8] However, WO_3 needed for WS_2 has a high bond energy and

sublimates at temperatures higher than 900 °C, which is less practical than MoO_3. Song et. al deposited thin WO_3 films by ALD at 300 °C and sulfurized these films afterwards at 1000 °C.[26] However, the sulfurization of WO_3 requires those high temperatures to enable the oxygen-sulfur exchange reaction in this oxide with high bond energy.[27], [28] We studied in this work an alternative approach, in which the tungsten is sulfurized directly from the metallic state. Normally, a metallic layer is difficult to maintain during the transport of a substrate in air. Therefore, the deposition is done in-situ in one reactor without vacuum break to avoid oxidation. In this paper we elaborate on the process described earlier, in which we convert an amorphous silicon film by WF_6 into metallic W and convert it in situ into WS_2 at a moderate processing temperature of 450 °C in H_2S.[29], [30] This study discusses the detailed observations of the formation mechanisms, namely the Si-to-W conversion and the sulfurization directly from metallic W to WS_2. The necessity for the surface preparation and restrictions with regards to thickness control, temperature, and structure are discussed.

The selective deposition of W on Si surfaces by CVD is a well-known process, which is mainly used for W-plug formation in vertical interconnect accesses (VIA) in combination with a Ti buffer layer.[31]–[33] In contrast, the W deposition on dielectric surfaces is more challenging due to the lack of potential nucleation sites. The formation of a thin W film from the precursor WF_6 on dielectrics such as Al_2O_3, HfO_2, or SiN requires the use of a reductant, since these dielectrics do not provide chemisorption sites for the precursor. Successful nucleation could be achieved by the use of H_2 plasma[29] or gases like Si_2H_6[34], SiH_4[35], B_2H_6[36], GeH_4[37], or solids like elemental Si[38], [39]. The aforementioned gaseous precursors are used for ALD processes to achieve layer-by-layer deposition of amorphous or polycrystalline

films. However, they deposit the target material on the whole substrate and not in specific regions. Nonetheless, a solid precursor like a thin Si film can be pre patterned and controls the areas for the conversion.

In contrast to the above described methods, the technique developed in this paper allows the selective deposition of WS_2 with arbitrary thickness equivalent to multilayer thickness down to a monolayer over wafer sizes of 300 mm diameter and exploits conventional tools for CMOS fabrication such as physical vapor deposition (PVD), wet chemical processing, and CVD. Here we provide insight into the conversion mechanisms with a focus on surface preparation, conversion temperature, and thickness correlation.

This conversion process can be used in combination with advanced techniques such as atomic layer etching (ALEt) to form selectively grown patterns on sensitive underlying films bringing advanced Beyond Si-CMOS concepts, such as tunnel field-effect transistors (TFET) or spintronic devices a step closer.

Methods

Substrates used in this work were 300 mm Si wafers coated with a 20 nm-thick thermally grown SiO_2 layer to provide interference contrast for 2D material visibility. This SiO_2 was covered by an atomic layer-deposited (ALD) Al_2O_3 and crystallized in O_2-rich environment at 1000 °C to chemically mimic a sapphire surface and to protect the Si wafer from reactions with the used gas phase precursor or wet-chemical surface preparations.

Amorphous silicon layers were deposited by PVD with a low deposition rate of 6.8 Å/min. This amorphous silicon is a uniform, sacrificial layer and used as reductant, i.e. it is consumed during the proceeding steps. The native SiO_2 was removed and Si was H-passivated by a 200 s long 0.5 % HF rinse and followed by an extensive H_2O rinse. These layers were immediately exposed to alternating gas pulses of WF_6 and H_2S in a CVD reactor at a temperature of 450 °C according to the scheme shown in Figure 1.
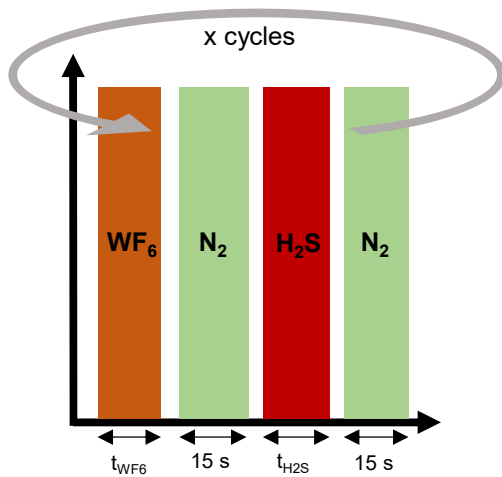

Figure 1: Pulse sequence in the CVD reactor with varying pulse times t, separated by 15 s N_2 purge steps

This converted the Si film into metallic W and subsequently into WS_2. The 15 s long gas pulses were separated by N_2 purges. The pressure was kept constant at 266 Pa. The conversion mechanism was thoroughly analyzed by Rutherford backscattering spectrometry (RBS) using 1.523 MeV He^+ particles.[40] Raman spectra were measured by a Horiba LabRAM HR with 532 nm excitation wavelength and a grating of 1800 grooves/mm. Angle-resolved X-ray photoelectron spectroscopy (AR-XPS) spectra were acquired with a ThermoInstruments Theta300 system using a monochromatized Al K_α X-ray source (1486.6 eV) and all spectra

were integrated over their measurement angles to obtain a high signal-to-noise ratio. Atomic force microscopy (AFM) by a Bruker Dimension ICON PT was used in tapping mode to collect information about the surface roughness. Selected samples were coated with spin-on-carbon (SOC) and cut with a 5 kV Ga^+ focused ion beam (FIB) into transmission-electron microscopy (TEM) specimens and then observed by a FEI Titan3 G2 60-300 with a Super-X EDS detector system. Grazing incidence X-ray diffraction spectra were recorded by a Panalytical X'PERT Pro MPD using an incidence angle of 1°.
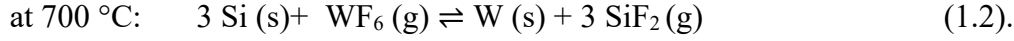
Results and Discussion

The deposition of WS_2 from gas phase precursors proceeds in two steps, the Si conversion to ultrathin, metallic W layers and the sulfurization of those metallic layers to WS_2. The following section discusses the impact of surface oxidation and the requirements for the Si surface preparation and the quantification of the conversion process from Si to W. Afterwards, the sulfurization and its constraints with respect to penetration depth and temperature are explained. After analyzing both processes separately, the combination was optimized to obtain stoichiometric films on an insulating substrate.

Redox reactions based on Si, WF_6, and H_2S

Si conversion to W: Role of surface passivation

Depending on the temperature, gaseous WF_6 reacts with Si according to the following paths by the up-diffusion of Si through thin W and reaction with the gaseous precursor at the surface:[41]

At 400 °C: $3\ \text{Si (s)} + 2\ \text{WF}_6\ \text{(g)} \rightleftharpoons 2\ \text{W (s)} + 3\ \text{SiF}_4\ \text{(g)}$ (1.1) or

at 700 °C: $3\ \text{Si (s)} + \text{WF}_6\ \text{(g)} \rightleftharpoons \text{W (s)} + 3\ \text{SiF}_2\ \text{(g)}$ (1.2).

Wafers with 7.5 Å-thick Si were exposed to the WF_6 at 450 °C after different periods upon Si deposition and the deposited W amount was quantified by RBS. The expected value for the number of W atoms per area N_W/A in the case of full conversion was calculated by

$$\frac{N_W}{A} = \frac{x}{3} \cdot \frac{N_{Si}}{A} = \frac{x \cdot \rho_{Si} \cdot N_A \cdot t_{Si}}{3 \cdot M_{Si}}$$ (1.3)

with the reaction coefficient x for W (either 2 or 1 for equation 1.1 or 1.2, respectively), the pre-deposited Si thickness t_{Si} and the corresponding number of Si atoms per area N_{Si}/A. The amorphous Si density ρ_{Si} can vary between 1.7 and 2.3 g/cm^3 depending on the deposition conditions.[42] With the molar mass M_{Si}, the theoretical density of W after full conversion for reaction 1.1 is in the range of 1.83E15 to 2.47E15 at/cm^2 and for reaction 1.2 it would yield only between 0.91E15 and 1.23E15 at/cm^2. Experimentally the 7.5 Å Si after conversion yielded 2.47E15 at/cm^2 This confirms that reaction 1.1 with the coefficient x = 2 occurred and the Si density of the pre deposited Si of silicon is similar to the crystalline density.

However, this amount was only achieved when the conversion with WF_6 was done immediately after the Si deposition. With increasing delay between the Si deposition and the conversion, less Si was converted to W for a similar Si amount, as shown in Figure 2. This is related to the formation of native SiO_2, of which the thickness is time-dependent.
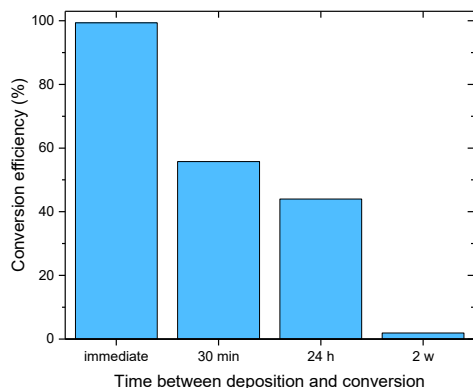
Figure 2: Conversion efficiency upon different periods between Si deposition and WF$_6$ conversion indicate a decreasing W amount. 100 % correspond to 2.47E15 at/cm^2

The amorphous Si forms a native oxide in air of a few Å. The exact thickness of this native oxide depends on the residence time in air.[43] Upon immediate WF$_6$ exposure for t_{WF6} = 15 s, the nominal Si amount of 7.5 Å resulted in nearly full conversion, whereas after 30 min only 55 % of the expected value was observed, after 24 h only 43 %, and upon two weeks delay, the deposited W amount was only 2 % of the expected value of full conversion.

This reveals the decreasing efficiency of Si-to-W conversion with increasing air exposure time. This observation can be explained by the non-reactivity of WF$_6$ and SiO$_2$ at the processing temperature of 450 °C.[44] It is therefore essential to carefully control the native oxide growth to avoid variability in W deposition. Samples treated with 14 cycles starting with t_{WF6} = 15 s WF$_6$ exposure but 24 h after Si deposition, show residual Si-O in the converted film according to XPS (Figure 3a), confirming the strongly limited reactivity of SiO$_2$ with WF$_6$. The SiO$_2$ is represented as the high energetic peak in the Si 2p spectra. In contrast to this, elemental Si being located at lower binding energy could not be quantified and only noise level was detected in this part of the spectrum, hence all elemental Si was consumed in the conversion process.

Correspondingly, reaction 1.1 occurred even through a thin native SiO_2 layer, which is not fully closed yet after short delay.

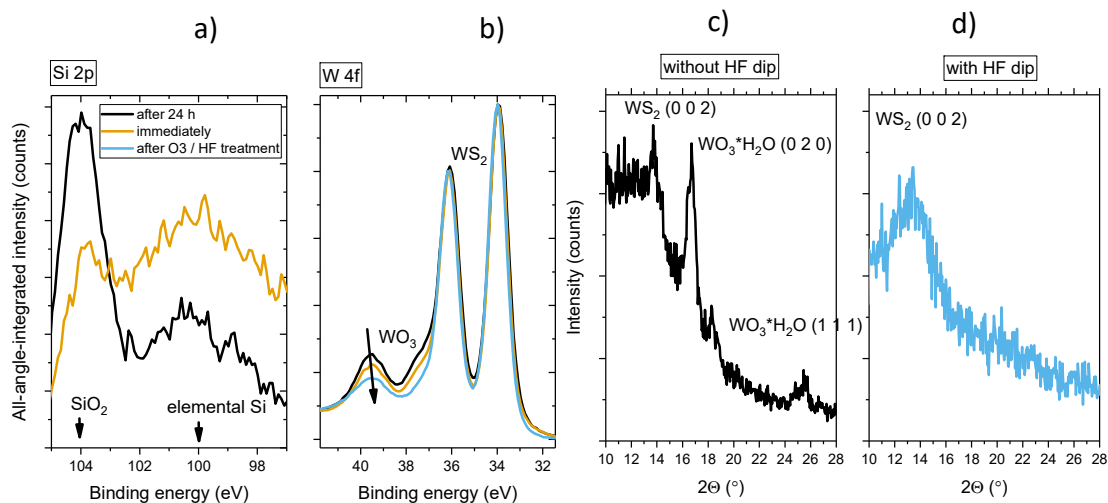Figure 3: XPS spectra of a) Si and b) W after immediate and one day-delayed treatment by the gas sequence WF_6, N_2, H_2S, N_2. The sample treated after one day shows the incorporation of SiO_2 from the native oxide, which was not converted into W-compound. GIXRD graphs showing the W-compounds deposited upon $WF_6/N_2/H_2S/N_2$ pulses on a sample with c) oxidized surface and on d) HF-cleaned surface. The latter one shows pure WS_2 formation and absence of tungstite.

Further analysis of the XPS spectra shown in Figure 3b revealed that oxygen was incorporated in the deposited W-compound. The spectrum shows two doublets of the W 4f peak: the lower energetic doublet is related to the W-S bonds, thus it represents the +IV oxidation state of W, which is typically related to WS_2.[45], [46] At higher binding energy, there is the W 4f doublet for WO_3 – this corresponds to W in the +VI oxidation state. This doublet is superimposed to the W 5p peak at the binding energy at 39.5 eV in this spectrum. The oxide can be distinguished qualitatively from the pure compound by the evolving shoulder next to the WS_2 doublet, which is part of the oxide characteristic doublet.

The quantitative oxide fraction of the deposited film was 16 % for the immediate conversion and 19 % for the conversion after 24 h (only partially converted). Both observations show higher oxidation than the typical 10 – 12 % oxidation (full conversion) we observe for the best material, probably originating from minor air oxidation. Typically, S-saturated W atoms oxidize only slowly under dry conditions and are stable for short-term as long as no elevated temperatures or moisture is applied for longer time.[47] The observed WO_3 oxidation implies that another oxygen source is present.

To identify this source, the composition was further analyzed upon deposition. The spectra in Figure 3b reveal a higher oxidation level in the film converted after 24 h in comparison to the one which was immediately converted. In addition, GIXRD spectra acquired upon deposition (Figure 3c) revealed significant peaks at 16.5 ° and 25.4 ° being characteristic for tungstite, $WO_3 \cdot H_2O$. This implies that the reaction product results from the interaction of SiO_2, WF_6, and air environment upon processing. SiO_2 cannot be directly etched by WF_6 due to its selectivity.[44], [48] However, WF_6 reacts with Si by penetrating through pinholes in the not fully closed native oxide layer, if this is still thin when it is only a few hours old. This forms SiF_4 as byproduct according to reaction 1.1, leading to the formation of a volatile silicon oxyfluoride according to 1.4 [49]:

$$3\ SiF_4\ (g) + SiO_2\ (s) \rightleftharpoons\ 2\ Si_2OF_6\ (g) \hspace{3cm} (1.4)$$

The O-containing reaction product from 1.4 is detracted by further reaction with WF_6 in the gas phase forming the metal-oxide compound according to the exergonic reaction ($\Delta G = -300$ kJ/mol):

$$3 \ Si_2OF_6 \, (g) + WF_6 \, (g) \rightleftharpoons WO_3 + 6 \ SiF_4 \, (g) \quad\quad\quad (1.5)$$
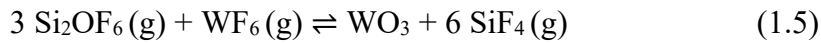
The oxygen of Si_2OF_6 could react with WF_6 due to the high affinity between both according to reaction 1.5. Upon air exposure, the incorporated oxide can hydrate and form the tungstite as evidenced in Figure 3c. To avoid the formation of tungstite and to achieve pure, oxygen-free WS_2, the incorporation of any oxygen on the sample surface has to be avoided. The challenges of preparing an O-free surface are twofold: on the one hand, the oxide regrowth on deposited Si is time-dependent and hence, it can vary depending on the time between Si deposition and oxide removal. As a result, the amount of elemental Si left is also time-dependent. On the other hand, the oxide regrowth should be avoided to minimize the adsorption of O_2 or H_2O prior to the W-compound deposition step. To tackle the first challenge of time-dependent oxidation, a chemical oxide based on ozonated H_2O was grown on the Si surface to achieve repeatable, constant Si consumption.[50] Afterwards, 0.5 % HF was applied for 200 s to remove the native/chemical oxide and then followed by an extensive H_2O rinse to passivate the surface with hydrogen, resulting in a hydrophobic surface that remains stable for extended periods of time.[51]

As the GIXRD spectra in Figure 3d show, the tungstite peaks are absent for the samples, which received the treatment of chemical oxidation and HF before the conversion process and only tungstenite is visible at 14 °. Additionally, the XPS spectra in Figure 3b reveal that the WO_3-related doublet diminishes and only the W 5f peak at high binding energy remains. According to the XPS quantification procedure, the remaining oxidation level of W-bonds is 12 %, which is the lowest value we obtain for any 2D material grown in our laboratory and that we could measure by ex situ analysis. By combination of ozonation and HF treatment the surface oxide

can be controlled and removed in a reproducible way leading to a stable H-passivated Si which can be used as a vehicle to study the conversion mechanism.

This conversion reaction was described earlier for W CVD deposition by the upward diffusion of Si through the growing W layer.[41] The segregated Si on top can react with the gaseous precursor, forms volatile SiF_4, and deposits the metallic W layer.

The film was exposed to 3 s WF_6 and a W amount of 2.5E+15 at/cm^2 was achieved. Saturation was observed after 15 s exposure as can be seen from Figure 4a. The XPS spectra in Figure 4b show remaining elemental Si and SiO_2 after the unsaturated 3 s WF_6 pulse and a Si-free surface for larger doses. This means that the dose for 3 s was too small to convert all the Si, whereas the 15 s are sufficient for converting all Si into W without any residual Si or SiO_2 incorporated.
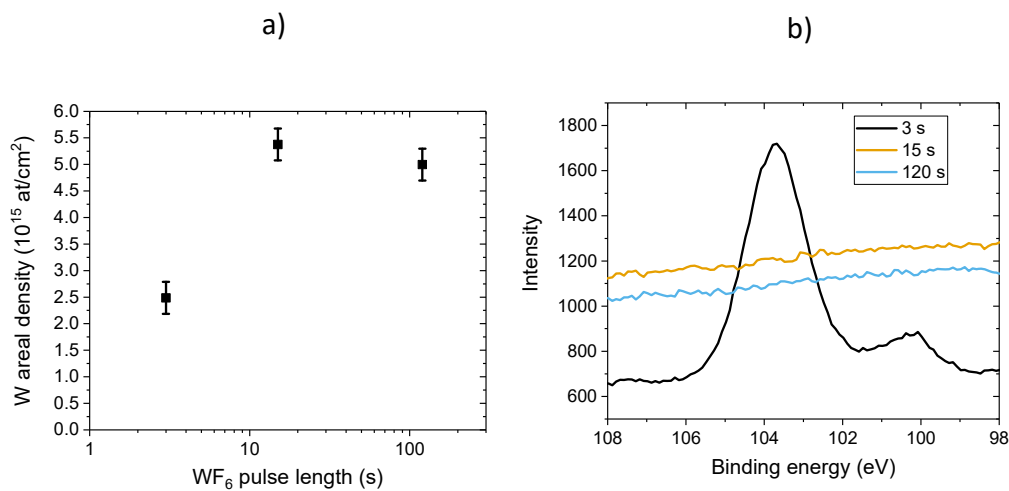
a)   b)

Figure 4: a) W after the conversion for different WF_6 exposure times; b) Si 2p XPS peak after different WF_6 exposure times shows that for the 3 s WF_6 not all the Si is consumed, whereas after 15 s and longer conversion, all Si above detection limit is consumed

Afterwards Si layers with different thicknesses were prepared and converted to W. The linear relationship between the deposited W amount and the pre deposited Si is depicted in Figure 5.

The intersection with the abscissa (1 nm) represents the amount of silicon which was consumed during the O_3 / H_2O oxidation and the HF-based SiO_2 removal. The slope derived from the linear fit is 2.51E15 at/cm²/nm. The linear correlation between W and Si and the absence of any residual Si (Fig. 2b) demonstrate the complete conversion of Si into W at 450 °C and in this way allows a precise controllability of the deposited amount.
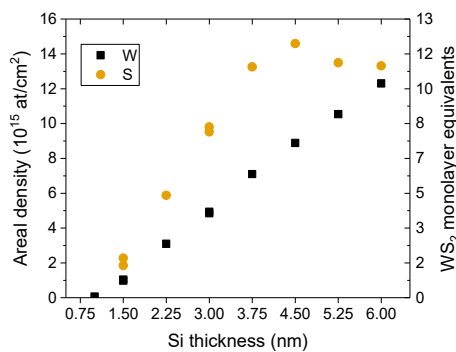

Figure 5: Deposited tungsten and sulfur amount as a function of the pre deposited Si thickness. Quantified by RBS.

WF_6 does not react with the crystallized Al_2O_3 underlayer as long as no other reductant is provided illustrating that this Si-to-W conversion process is selective as demonstrated in an earlier paper.[30]

Sulfurization reaction for the conversion of W to WS_2

After determining the parameters for a complete conversion of the pre deposited Si amount, the parameters of the sulfurization pulse were studied to obtain a stoichiometric WS_2. Obviously, this sulfurization pulse was applied in situ to avoid air exposure of the formed metallic compound, since it would oxidize rapidly.[52]

The H_2S pulse converts the deposited material according to:

$$W\text{ (s)} + 2\text{ }H_2S\text{ (g)} \rightleftharpoons WS_2\text{ (s)} + 4\text{ }H_2\text{(g)} \qquad\qquad (1.6)$$
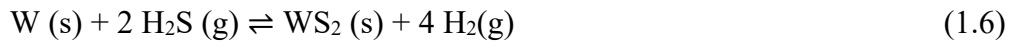
We can assume that all the initially deposited tungsten is in the metallic state, since the H_2S pulse is applied in situ and no O_2 is involved in any of the reactions after cleaning the surface properly. After a $t_{H2S} = 15$ s H_2S pulse at 450 °C, the sulfurization yielded only a S/W ratio of 1.5, hence the film was non-stoichiometric and only 75 % of the maximum sulfur amount was reached since the sulfurization reaction was not complete. A second cycle being equivalent to a dose for 30 s already increased the ratio to 1.7. Adding twelve more cycles with a total H_2S dosing of 210 s resulted in a S/W ratio of 1.8 and saturated around this level for a given initial Si thickness. This was equivalent to 90 % of the total theoretical sulfur amount.

Influence of the processing temperature

According to Figure 5, an initial Si thickness of 3 nm is necessary to realize a multilayer structure of four layers of WS_2. For this thickness, the temperature window was investigated. Figure 6a shows the S/W ratio after formation at various temperatures between 325 °C and 450 °C. With increasing temperature, the incorporated S amount is increasing as well and is reaching a S/W ratio close to 2 for 450 °C, but the W amount was constant for all three temperatures. The XPS spectra in Figure 6b show decreasing WO_3 doublets for increasing deposition temperatures, before reaching a minimum for 450 °C. We interpret the W-O oxide formation as saturation of metallic bonds upon air exposure, which is a different effect than shown before which was the oxide formation due to an oxide-contaminated surface of the Si precursor. When the sulfurization is conducted at 450 °C, a higher fraction of W is sulfurized and all the accessible W atoms are saturated with sulfur, so that the material is inert against

spontaneous oxidation in air. For T < 450 °C, the W films are not completely sulfurized and remaining W atoms oxidize in air.

The Raman spectra in Figure 6c show the characteristic peaks for WS_2: The higher the temperature, the higher are the intensities of the $2LA(M)/E^1_{2g}$ and A_{1g} peaks.[53] The overlapping peaks $2LA(M)$ and E^1_{2g} describe the second order Raman resonance peak of the longitudinal acoustic mode and the in-plane vibrational modes, respectively. The A_{1g} peaks describe the out-of-plane vibrational modes of the W-S bonds. Note how in contrast, the intensity of the Si 2TA mode at 300 cm^{-1} coming from the substrate remains relatively constant. Together with the rising LA(M) mode, often referred to as a measure for the disorder in MX_2 films, this can be interpreted as an increase in the WS_2 amount.[54]

These observations show that for T $\geq$ 325 °C, the limiting step is the sulfurization. For a given temperature, sufficiently long dosing of H_2S had to be provided to convert the thickness of a four layer-equivalent film. This is due to the diffusion of the reactant H_2S through the top layer of WS_x and the out-diffusion of the reaction product H_2 according to reaction 1.6. Diffusion is a temperature-determined process and thus, higher temperatures allow deeper diffusion of sulfur for a given reaction time.

At 450 °C the conversion of a 3 nm-thick Si and the stoichiometric sulfurization of the W could be achieved. This temperature was used in all the following experiments to obtain stoichiometric films.
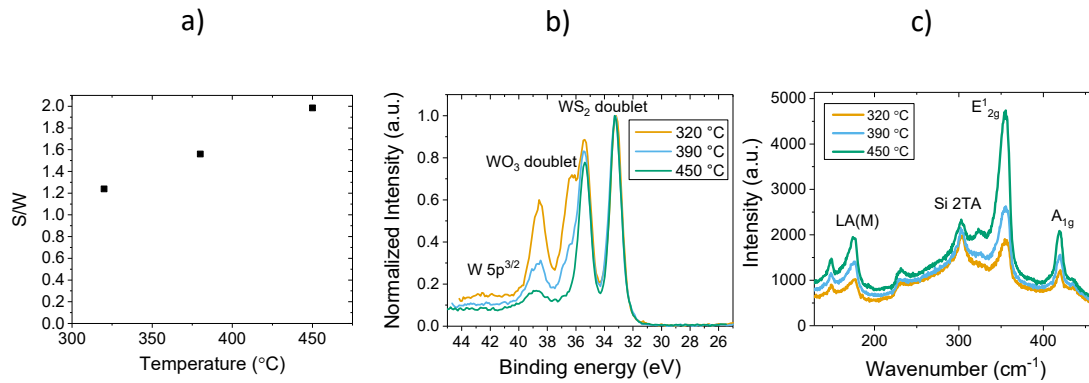
a)   b)   c)

Figure 6: a) S and W amount as determined by RBS showing that stoichiometric films can only be obtained at 450 °C; b) XPS spectra of the W region reveal the presence of WS_2 and WO_3. The WO_3 contribution disappeared for the 450 °C process; c) Raman spectra taken upon WS_2 deposition show an increase in the $2LA(M)/E^1_{2g}$ and A_{1g} peak for higher deposition temperatures

Influence of the starting Si thickness for controllability of layers

The properties of 2D materials vary significantly with the thickness and the optimal thickness for MX_2 transistors remains under debate.[55], [56] In the following we evaluated whether the WS_2 thickness could be modulated by the amount of pre deposited Si.

To achieve the deposition of different thicknesses of stoichiometric WS_2 films, Si films with different thicknesses were pre deposited and converted to WS_2 with $t_{WF6} = t_{H2S} = 15$ s long pulses at 450 °C. The amount of W and S was quantified as shown in Figure 5.
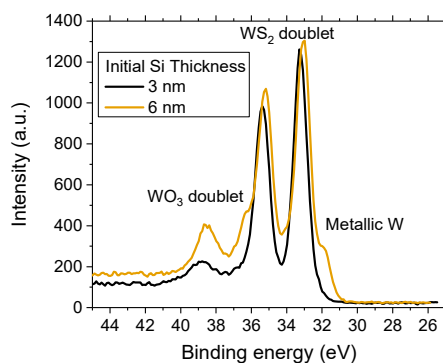
Figure 7: XPS spectra with the W-related peaks of a thin and a thick film. The thicker film shows stronger oxidation on the top and a buried metallic contribution, which is not present in the thinner film.

While the W amount increases linearly with the amount of pre deposited Si, the S amount increases linearly up to ~3.75 nm Si and then saturates, there is no more sulfur incorporation above this amount. This is related to the limited H_2S diffusion into the deposited film at the temperature used.[57], [58] Since the conversion Si →W is done in situ with the H_2S sulfurization, both cycles are conducted at the same temperature. H_2S has to penetrate through the surface layer, react with the metal underneath, and H_2 as reaction product has to diffuse out of the films. The 450 °C process is capable of sulfurizing one to six layers at the given H_2S dose and temperature. If the films become too thick, the H_2S is not capable of diffusing deep enough, which can be seen by residual metallic W in the XPS spectra in Figure 7. There is also an increased WO_3 amount appearing, being buried at the interface between the sulfur-terminated W-S and the metallic W. This WO_3 is formed due to non-reacted W, which is brought into contact with O_2 from the atmosphere. Hence, at room temperature O_2 can still diffuse through the top layer oxidizing a part of the metallic W underneath, which can be

understood from the smaller van-der-Waals radius of oxygen of 1.52 Å with respect to the larger one of sulfur with 1.80 Å. Thus, O_2 is assumed to penetrate deeper than H_2S at low temperatures. Diffusion is a temperature-controlled mechanism, therefore only higher temperatures or longer annealing periods could sulfurize thicker layers, but this is out of the range of the available experimental setup and also not targeted for the application in few-layered active films.

Necessity of a cycled process

Introducing the gas pulses sequentially with a saturated WF_6 pulse for conversion and at least partial sulfurization is essential due to the interaction of the solid and gas compounds. We tested the hypothesis whether a partial conversion by a short WF_6 pulse, followed by a long sulfurization step could result in smaller nucleation density and facilitate large crystal growth from fewer nuclei by repeating such cycles. However, we observed that after the first unsaturated WF_6 pulse and the H_2S pulse, no further conversion of Si into W occurred after the second WF_6 cycle, as WF_6 cannot reach the elemental Si underneath anymore and the Si does not diffuse upward through the WS_2. In contrast, the sulfurization reaction continues in the second cycle. Hence the formed WS_2 top layer act as a barrier and prevents the further upward diffusion of Si through the WS_2 film and the Si interaction with WF_6.

The *simultaneous* injection of WF_6 and H_2S was investigated on the H-terminated Si (CVD regime). We observed the formation of a film with monolayer-equivalent thickness being also stoichiometric. However, the thickness of this film did not scale with deposition time. In this case the surface reaction took place as well, but further surface reaction was strongly reduced and

formation of a second layer occurred only very slowly, since the top surface WS_2 film prevented any further exchange between the buried reductant silicon and the gaseous WF_6.

The goal of this work is the deposition of TMD on the insulating substrate without leaving silicon traces behind. We conclude that it is necessary to first *fully* convert the Si into W, and only afterwards the sulfurization of the W film can be carried out.

Figure 8 shows a TEM cross-sectional image of a stoichiometric film deposited with optimized conditions. The image shows in the bottom part the polycrystalline Al_2O_3, in the middle the WS_2 films, and above the spin-on-carbon (SOC) capping layer. In the SOC layer some darker regions are visible, which represents driven-out sulfur by the sample preparation through focussed ion beam.
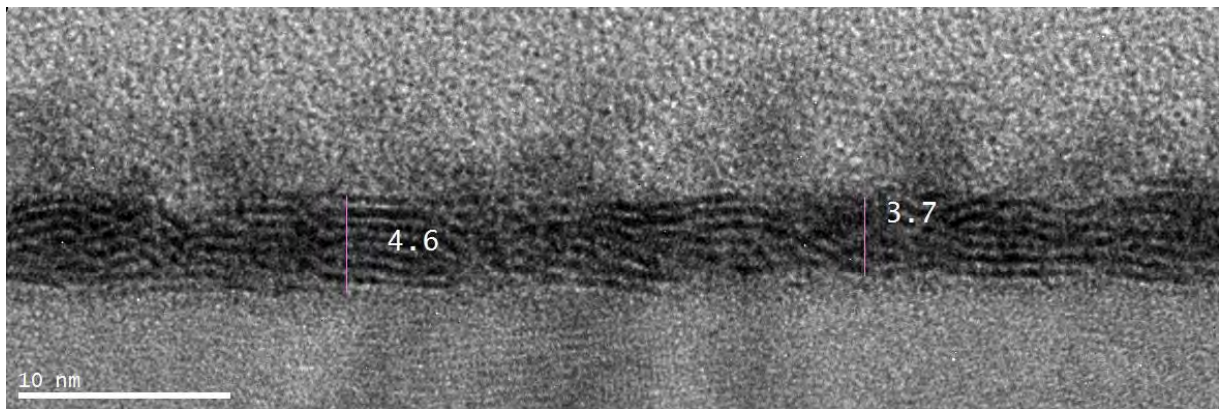

Figure 8: TEM cross-sectional image of a stoichiometric WS_2 film prepared with 14 cycles of ($WF_6/N_2/H_2S/N_2$ of 15 s period for each pulse). The bars with the numbers indicate the thickness of the WS_2 film in nm.

The layered structure of the W and S is visible, but with short-range order. The size of clusters with parallel basal plane structure is less than 3 nm and, in between, areas appear amorphous. The similar random orientation of WS_2 clusters was observed for different thicknesses and similar stoichiometry of the films. In case of thin non-stoichiometric films, the basal planes of

the clusters are rather vertically aligned and WO_3 clusters remain in the film. The stoichiometric films can be used for further recrystallization experiments, which is part of further research.[59], [60]

Conclusions

A method has been described, allowing to deposit one to six layers WS_2. The method starts from on amorphous Si, of which the thickness determines the amount of WS_2 to be formed. To obtain pure WS_2, the Si layer needs to be oxygen-free. Reproducible Si layers can be obtained by the oxidation with a H_2O-O_3 mixture and a subsequent HF treatment, which passivates the surface with H and delays re-oxidation. The silicon layers can be converted to metallic W with WF_6 at $T \geq 325$ °C, then in situ sulfurized by H_2S, which is energetically favorable over oxygen-sulfur exchange in WO_3 compounds. The formation of WS_2 creates a barrier against a subsequent Si / WF_6 exchange, which imposes that the starting Si film must be fully converted into W in the first cycle. The sulfurization step is a diffusion-driven process and is limited to a thickness equivalent of six layers WS_2 at 450 °C. The obtained WS_2 layers with random basal plane orientation can serve as template for subsequent recrystallization to obtain larger crystals. We believe that this technique can pave the way for a selective deposition on large substrates and could enable heterostructures for TFETs, spintronics, and optical applications.

Acknowledgement

Reference

[1]   S.-H. Lin and J.-L. Kuo, "Activating and tuning basal planes of MoO 2 , MoS 2 , and MoSe 2 for hydrogen evolution reaction," *Phys. Chem. Chem. Phys.*, vol. 17, no. 43, pp. 29305–29310, 2015.

[2]   L. Liu, Y. Lu, and J. Guo, "On Monolayer MoS2 Field-Effect Transistors at the Scaling Limit," *IEEE Trans. Electron Devices*, vol. 60, no. 12, pp. 4133–4139, Dec. 2013.

[3]   O. Lopez-Sanchez, D. Lembke, M. Kayci, A. Radenovic, and A. Kis, "Ultrasensitive photodetectors based on monolayer MoS2," *Nat. Nanotechnol.*, vol. 8, no. 7, pp. 497–501, Jun. 2013.

[4]   Y. K. Luo, J. Xu, T. Zhu, G. Wu, E. J. McCormick, W. Zhan, M. R. Neupane, and R. K. Kawakami, "Opto-valleytronic spin injection in monolayer MoS2/few-layer graphene hybrid spin valves," *Nano Lett.*, vol. 17, no. 6, pp. 3877–3883, 2017.

[5]   W. G. Song, H.-J. Kwon, J. Park, J. Yeo, M. Kim, S. Park, S. Yun, K.-U. Kyung, C. P. Grigoropoulos, S. Kim, and Y. K. Hong, "High-Performance Flexible Multilayer MoS2 Transistors on Solution-Based Polyimide Substrates," *Adv. Funct. Mater.*, vol. 26, no. 15, pp. 2426–2434, 2016.

[6]   K.-T. Chen and S.-T. Chang, "How high can the mobility of monolayer tungsten disulfide be?," *Vacuum*, vol. 140, pp. 172–175, Jun. 2017.

[7]   K. Chen and S. Chang, "Phonon limited electron mobility calculation of transition metal dichalcogenide monolayer," in *2016 IEEE 16th International Conference on Nanotechnology (IEEE-NANO)*, 2016, vol. 2, no. 1, pp. 139–141.

[8]   Y. Yoon, K. Ganapathi, and S. Salahuddin, "How good can monolayer MoS2 transistors be?," *Nano Lett.*, vol. 11, no. 9, pp. 3768–3773, 2011.

[9]   D. Chiappe, I. Asselberghs, S. Sutar, S. Iacovo, V. Afanas'ev, A. Stesmans, Y. Balaji, L. Peters, M. Heyne, M. Mannarino, W. Vandervorst, S. Sayan, C. Huyghebaert, M. Caymax, M. Heyns, S. De Gendt, I. Radu, and A. Thean, "Controlled Sulfurization Process for the Synthesis of Large Area MoS 2 Films and MoS 2 /WS 2 Heterostructures," *Adv. Mater. Interfaces*, vol. 3, no. 4, p. 1500635, Feb. 2016.

[10]   A. Zafar, H. Nan, Z. Zafar, Z. Wu, J. Jiang, Y. You, and Z. Ni, "Probing the intrinsic optical quality of CVD grown MoS2," *Nano Res.*, vol. 10, no. 5, pp. 1608–1617, May 2017.

[11]   S. Wang, Y. Rong, Y. Fan, M. Pacios, H. Bhaskaran, K. He, and J. H. Warner, "Shape evolution of monolayer MoS2 crystals grown by chemical vapor deposition," *Chem. Mater.*, vol. 26, no. 22, pp. 6371–6379, 2014.

[12]   Y. Kim, H. Bark, G. H. Ryu, Z. Lee, and C. Lee, "Wafer-scale monolayer MoS2 grown by chemical vapor deposition using a reaction of MoO3 and H2S," *J. Physics-Condensed Matter*, vol. 28, no. 18, p. 6, 2016.

[13]   Y.-H. Lee, X.-Q. Zhang, W. Zhang, M.-T. Chang, C.-T. Lin, K.-D. Chang, Y.-C. Yu, J. T.-W. Wang, C.-S. Chang, L.-J. Li, and T.-W. Lin, "Synthesis of large-area MoS2 atomic layers with chemical vapor deposition.," *Adv. Mater.*, vol. 24, no. 17, pp. 2320–5, May 2012.

[14]   Y. Zhang, Y. Zhang, Q. Ji, J. Ju, H. Yuan, J. Shi, T. Gao, D. Ma, M. Liu, Y. Chen, X. Song, H. Y. Hwang, Y. Cui, and Z. Liu, "Controlled growth of high-quality monolayer WS2 layers on sapphire and imaging its grain boundary," *ACS Nano*, vol. 7, no. 10, pp. 8963–8971, 2013.

[15]   L. Ma, D. N. Nath, E. W. Lee, C. H. Lee, M. Yu, A. Arehart, S. Rajan, and Y. Wu, "Epitaxial growth of large area single-crystalline few-layer MoS2 with high space charge mobility of 192 cm2 V−1 s−1," *Appl. Phys. Lett.*, vol. 105, no. 7, p. 72105, 2014.

[16]   K. Jung, C. Y. Liu, J. D. Kim, W. Choi, W. Zhou, H. C. Kuo, and X. Li, "Large area MoS2 van der Waals epitaxy on III-Ns and the epitaxial formation of a n-MoS2/p-InGaN diode," *2016 IEEE Photonics Conf. IPC 2016*, pp. 657–658, 2017.

[17]   D. Ruzmetov, K. Zhang, G. Stan, B. Kalanyan, G. R. Bhimanapati, S. M. Eichfeld, R. A. Burke, P. B. Shah, T. P. O'Regan, F. J. Crowne, A. G. Birdwell, J. A. Robinson, A. V. Davydov, and T. G. Ivanov, "Vertical 2D/3D Semiconductor Heterostructures Based on Epitaxial Molybdenum Disulfide and Gallium Nitride," *ACS Nano*, vol. 10, no. 3, pp. 3580–3588, 2016.

[18]   W. Y. Lee, T. M. Besmann, and M. W. Stott, "Preparation of MoS2 thin films by chemical vapor deposition," *J. Mater. Res.*, vol. 9, no. 6, pp. 1474–1483, Jun. 1994.

[19] I. Endler, A. Leonhardt, U. König, H. van den Berg, W. Pitschke, and V. Sottke, "Chemical vapour deposition of MoS_2 coatings using the precursors $MoCl_5$ and H_2S," *Surf. Coatings Technol.*, vol. 120–121, pp. 482–488, Nov. 1999.

[20] N. D. Boscher, C. J. Carmalt, R. G. Palgrave, J. J. Gil-Tomas, and I. P. Parkin, "Atmospheric Pressure CVD of Molybdenum Diselenide Films on Glass," *Chem. Vap. Depos.*, vol. 12, no. 11, pp. 692–698, Nov. 2006.

[21] Y. Jang, S. Yeo, H.-B.-R. Lee, H. Kim, and S.-H. Kim, "Wafer-scale, conformal and direct growth of MoS_2 thin films by atomic layer deposition," *Appl. Surf. Sci.*, vol. 365, pp. 160–165, Mar. 2016.

[22] S. H. Choi, B. Stephen, J.-H. Park, J. S. Lee, S. M. Kim, W. Yang, and K. K. Kim, "Water-Assisted Synthesis of Molybdenum Disulfide Film with Single Organic Liquid Precursor," *Sci. Rep.*, vol. 7, no. 1, p. 1983, 2017.

[23] S. Dhar, V. K. Kumar, T. H. Choudhury, S. A. Shivashankar, and S. Raghavan, "Chemical vapor deposition of MoS_2 layers from Mo-S-C-O-H system: thermodynamic modeling and validation," *Phys. Chem. Chem. Phys.*, vol. 18, no. 22, pp. 14918–14926, 2016.

[24] C. Gas, P. Decomposition, M. R. Close, J. L. Petersen, and E. L. Kugler, "Synthesis and Characterization of Nanoscale Molybdenum Sulfide Catalysts by Controlled Gas Phase Decomposition of $Mo(CO)_6$ and H_2S," *Inorg. Chem.*, vol. 38, no. 7, pp. 15–34, Apr. 1999.

[25] M. H. Heyne, D. Chiappe, J. Meersschaut, T. Nuytten, T. Conard, H. Bender, C. Huyghebaert, I. P. Radu, M. Caymax, J.-F. de Marneffe, E. C. Neyts, and S. De Gendt,

"Multilayer MoS 2 growth by metal and metal oxide sulfurization," *J. Mater. Chem. C*, vol. 4, no. 6, pp. 1295–1304, 2016.

[26] J. G. Song, J. Park, W. Lee, T. Choi, H. Jung, C. W. Lee, S. H. Hwang, J. M. Myoung, J. H. Jung, S.-H. H. Kim, C. Lansalot-Matras, and H. Kim, "Layer-controlled, wafer-scale, and conformal synthesis of tungsten disulfide nanosheets using atomic layer deposition," *ACS Nano*, vol. 7, no. 12, pp. 11333–40, Dec. 2013.

[27] T. Weber, J. C. Muijsers, J. H. M. C. van Wolput, C. P. J. Verhagen, and J. W. Niemantsverdriet, "Basic Reaction Steps in the Sulfidation of Crystalline MoO 3 to MoS 2 , As Studied by X-ray Photoelectron and Infrared Emission Spectroscopy," *J. Phys. Chem.*, vol. 100, no. 33, pp. 14144–14150, Jan. 1996.

[28] A. Van der Vlies, A. J. van der Vlies, R. Prins, and T. Weber, "Chemical Principles of the Sulfidation of Tungsten Oxides," *J. Phys. Chem. B*, vol. 106, no. 36, pp. 9277–9285, Sep. 2002.

[29] A. Delabie, M. Caymax, B. Groven, M. Heyne, K. Haesevoets, J. Meersschaut, T. Nuytten, H. Bender, T. Conard, P. Verdonck, S. Van Elshocht, S. De Gendt, M. Heyns, K. Barla, I. Radu, and A. Thean, "Low temperature deposition of 2D WS 2 layers from WF 6 and H 2 S precursors: impact of reducing agents," *Chem. Commun.*, vol. 51, no. 86, pp. 15692–15695, 2015.

[30] M. H. Heyne, J.-F. de Marneffe, A. Delabie, M. Caymax, E. C. Neyts, I. Radu, C. Huyghebaert, and S. De Gendt, "Two-dimensional WS 2 nanoribbon deposition by conversion of pre-patterned amorphous silicon," *Nanotechnology*, vol. 28, no. 4, p.

04LT01, Jan. 2017.

[31] E. K. Broadbent, "Selective Low Pressure Chemical Vapor Deposition of Tungsten," *J. Electrochem. Soc.*, vol. 131, no. 6, p. 1427, 1984.

[32] J. Carlsson and M. Boman, "Selective deposition of tungsten—prediction of selectivity," *J. Vac. Sci. Technol. A Vacuum, Surfaces, Film.*, vol. 3, no. 6, pp. 2298–2302, 1985.

[33] Y. Pauleau, P. Lami, A. Tissier, R. Pantel, and J. C. Oberlin, "Tungsten films produced by selective deposition onto silicon wafers," *Thin Solid Films*, vol. 143, no. 3, pp. 259–267, Oct. 1986.

[34] R. K. Grubbs, C. E. Nelson, N. J. Steinmetz, and S. M. George, "Nucleation and growth during the atomic layer deposition of W on Al2O3 and Al2O3 on W," *Thin Solid Films*, vol. 467, no. 1–2, pp. 16–27, 2004.

[35] B. Kalanyan, P. C. Lemaire, S. E. Atanasov, M. J. Ritz, and G. N. Parsons, "Using Hydrogen To Expand the Inherent Substrate Selectivity Window During Tungsten Atomic Layer Deposition," *Chem. Mater.*, vol. 28, no. 1, pp. 117–126, Jan. 2016.

[36] G. Wang, Q. Xu, T. Yang, J. Luo, J. Xiang, J. Xu, G. Xu, C. Li, J. Li, J. Yan, C. Zhao, D. Chen, and T. Ye, "Application of Atomic Layer Deposition Tungsten (ALD W) as Gate Filling Metal for 22 nm and Beyond Nodes CMOS Technology," *ECS Trans.*, vol. 58, no. 10, pp. 317–324, Aug. 2013.

[37] G. J. Leusink, T. G. M. Oosterlaken, G. C. A. M. Janssen, and S. Redelaar, "Chemical vapour deposition tungsten film growth studied by in situ growth stress measurements,"

Thin Solid Films, vol. 228, no. 1–2, pp. 125–128, May 1993.

[38]   J. C. Dupuy, A. Essaadani, A. Sibai, C. Dubois, F. C. Dassapa, and Y. Pauleau, "SIMS depth profiles study of W☐Si structures produced via the silicon reduction of tungsten hexafluoride," *Thin Solid Films*, vol. 227, no. 2, pp. 167–176, May 1993.

[39]   M. L. Green, "The Formation and Structure of CVD W Films Produced by the Si Reduction of WF[sub 6]," *J. Electrochem. Soc.*, vol. 134, no. 9, p. 2285, 1987.

[40]   J. Meersschaut and W. Vandervorst, "High-throughput ion beam analysis at imec," *Nucl. Instruments Methods Phys. Res. Sect. B Beam Interact. with Mater. Atoms*, vol. 406, pp. 25–29, 2017.

[41]   M. L. Yu, K. Y. Ahn, and R. V. Joshi, "Surface chemistry of the WF$_6$-based chemical vapor deposition of tungsten," *IBM J. Res. Dev.*, vol. 34, no. 6, pp. 875–883, Nov. 1990.

[42]   O. Renner and J. Zemek, "Density of amorphous silicon films," *Czechoslov. J. Phys.*, vol. 23, no. 11, pp. 1273–1276, Nov. 1973.

[43]   M. Morita, T. Ohmi, E. Hasegawa, M. Kawakami, and M. Ohwada, "Growth of native oxide on a silicon surface," *J. Appl. Phys.*, vol. 68, no. 3, pp. 1272–1281, Aug. 1990.

[44]   A. Kepten, "Studies of the Possible Reaction of WF[sub 6] with SiO[sub 2] and Si[sub 3]N[sub 4] at Several Temperatures," *J. Electrochem. Soc.*, vol. 139, no. 8, p. 2331, 1992.

[45]   P. C. Yen, Y. S. Huang, and K. K. Tiong, "The growth and characterization of rhenium-doped WS2 single crystals," *J. Phys. Condens. Matter*, vol. 16, no. 12, pp. 2171–2180,

2004.

[46]   X. Mao, Y. Xu, Q. Xue, W. Wang, and D. Gao, "Ferromagnetism in exfoliated tungsten

disulfide nanosheets.," *Nanoscale Res. Lett.*, vol. 8, no. 1, p. 430, Jan. 2013.

[47]   J. Gao, B. Li, J. Tan, P. Chow, T. M. Lu, and N. Koratkar, "Aging of Transition Metal

Dichalcogenide Monolayers," *ACS Nano*, vol. 10, no. 2, pp. 2628–2635, 2016.

[48]   F. R. McFeely, L. J. Terminello, and S. P. Kowalczyk, "Comparison of the selective

adsorption and reactivity behavior of WF 6 and TaF 5 on SiO 2 and polyimide surfaces,"

Appl. Phys. Lett., vol. 57, no. 7, pp. 667–669, Aug. 1990.

[49]   M. Shinmei, T. Imai, T. Yokokawa, and C. . Masson, "Thermodynamic study of

Si2OF6(g) from 723 to 1288 K by mass spectrometry," *J. Chem. Thermodyn.*, vol. 18, no.

3, pp. 241–246, Mar. 1986.

[50]   F. De Smedt, C. Vinckier, I. Cornelissen, S. De Gendt, and M. Heyns, "A Detailed Study

on the Growth of Thin Oxide Layers on Silicon Using Ozonated Solutions," *J.

Electrochem. Soc.*, vol. 147, no. 3, p. 1124, 2000.

[51]   H. Bender, "Hydrogen Passivation of HF-Last Cleaned (100) Silicon Surfaces

Investigated by Multiple Internal Reflection Infrared Spectroscopy," *J. Electrochem. Soc.*,

vol. 141, no. 11, p. 3128, 1994.

[52]   A. Warren, A. Nylund, and I. Olefjord, "Oxidation of tungsten and tungsten carbide in dry

and humid atmospheres," *Int. J. Refract. Met. Hard Mater.*, vol. 14, no. 5–6, pp. 345–353,

1996.

[53] A. Berkdemir, H. R. Gutiérrez, A. R. Botello-Méndez, N. Perea-López, A. L. Elías, C.-I. Chia, B. Wang, V. H. Crespi, F. López-Urías, J.-C. Charlier, H. Terrones, and M. Terrones, "Identification of individual and few layers of WS2 using Raman Spectroscopy," *Sci. Rep.*, vol. 3, p. 1755, Apr. 2013.

[54] S. Mignuzzi, A. J. Pollard, N. Bonini, B. Brennan, I. S. Gilmore, M. A. Pimenta, D. Richards, and D. Roy, "Effect of disorder on Raman scattering of single-layer Mo S2," *Phys. Rev. B - Condens. Matter Mater. Phys.*, vol. 91, no. 19, pp. 1–7, 2015.

[55] J. H. Kim, T. H. Kim, H. Lee, Y. R. Park, W. Choi, and C. J. Lee, "Thickness-dependent electron mobility of single and few-layer MoS 2 thin-film transistors," *AIP Adv.*, vol. 6, no. 6, p. 65106, Jun. 2016.

[56] M.-W. Lin, I. I. Kravchenko, J. Fowlkes, X. Li, A. A. Puretzky, C. M. Rouleau, D. B. Geohegan, and K. Xiao, "Thickness-dependent charge transport in few-layer MoS 2 field-effect transistors," *Nanotechnology*, vol. 27, no. 16, p. 165203, Apr. 2016.

[57] P. Si, M. Zhang, Z. Zhang, X. Zhao, and X. Ma…, "Synthesis and structure of multi-layered WS2 (CoS), MoS2 (Mo) nanocapsules and single-layered WS2 (W) nanoparticles," *J. Mater. … VN - readcube.com*, vol. 0, pp. 4287–4291, 2005.

[58] M. H. Heyne, D. Chiappe, J. Meersschaut, T. Nuytten, T. Conard, H. Bender, C. Huyghebaert, I. P. Radu, M. Caymax, J.-F. De Marneffe, E. C. Neyts, and S. De Gendt, "Multilayer MoS<inf>2</inf> growth by metal and metal oxide sulfurization," *J. Mater. Chem. C*, vol. 4, no. 6, 2016.

[59] J. J. Pyeon, S. K. S. H. Kim, D. S. Jeong, S.-H. Baek, C.-Y. Kang, J.-S. Kim, and S. K. S.

H. Kim, "Wafer-scale growth of MoS 2 thin films by atomic layer deposition," *Nanoscale*, vol. 8, no. 20, pp. 10792–10798, 2016.

[60]   J. H. Huang, K. Y. Deng, P. S. Liu, C. T. Wu, C. T. Chou, W. H. Chang, Y. J. Lee, and T. H. Hou, "Large-Area 2D Layered MoTe2 by Physical Vapor Deposition and Solid-Phase Crystallization in a Tellurium-Free Atmosphere," *Adv. Mater. Interfaces*, vol. 1700157, pp. 2–9, 2017.